Coinciding local bifurcations in the Navier-Stokes equations

Nan Deng, Luc Pastur, Laurette Tuckerman, Bernd Noack

Coinciding local bifurcations in the Navier-Stokes equations

Nan Deng[1], Luc R. Pastur[1], Laurette S. Tuckerman[2] and Bernd R. Noack[3]

[1] *Institute of Mechanical Sciences and Industrial Applications (IMSIA), ENSTA-Paris, Institut Polytechnique de Paris - 828 Bd des Maréchaux, F-91120 Palaiseau, France*
[2] *Laboratoire de Physique de Mécanique des Milieux Hétéerogènes (PMMH), CNRS, ESPCI Paris, PSL Research University; Sorbonne Université, Université de Paris - F-75005, Paris, France*
[3] *Center for Turbulence Control, Harbin Institute of Technology, Shenzhen Campus - University Town, Shenzhen 518058, People's Republic of China*

PACS 11.30.Qc – Symmetry breaking
PACS 47.20.Ky – Flow instabilities
PACS 47.15.Tr – Laminar wakes

Abstract – Generically, a local bifurcation only affects a single solution branch. However, branches that are quite different may nonetheless share certain eigenvectors and eigenvalues, leading to coincident bifurcations. For the fluidic pinball, two supercritical pitchfork bifurcations, of the equilibrium and the periodic solutions, occur at nearly the same Reynolds number. The mechanism of this kind of non-generic coincidence is modelled and explained.

Introduction. – Vortex shedding, symmetry breaking, and self-sustained oscillations are very common in fluid flows [1–3]. In terms of dynamical systems theory, vortex shedding in the wake of an obstacle usually results from a Hopf bifurcation, either supercritical, as in the cylinder wake flow [4, 5] and in the wake of axisymmetric bodies [6], or subcritical, as in a stalling wing [7]. Symmetry-breaking pitchfork bifurcations may also occur, again either supercritical, as in bluff body wake flows [8], or subcritical, as in a symmetric channel with an expanded and contracted section [9] and in spherical Couette flow [10]. Many shear flows at high Reynolds numbers feature coherent structures similar to the patterns engendered by instabilities of the basic flow at low Reynolds numbers. For instance, the von Kármán streets of vortices found in the wake of cylinders in cross-flow develop at Reynolds numbers as small as $O(10^2)$, where the flow is laminar, while the alley of vortices in the wake of islands in oceans are still observed for Reynolds numbers as large as $O(10^8)$, where the flow is fully turbulent. This is also true for the Kelvin-Helmholtz instability [11] and Taylor-Couette flow [12]. New states may arise via secondary instabilities of the basic flow as the Reynolds number is increased. Examples are the subcritical pitchfork bifurcation of turbulent vortex shedding [13] and secondary transitions of the cylinder wake [14, 15].

Generically, a local bifurcation only affects one solution branch (as its name implies) and cannot affect the stability of other solution branches. Quite intriguingly however, a recent study of the fluidic pinball configuration has shown that two local bifurcations occur almost simultaneously, i.e. at nearly the same critical Reynolds number [16]. Both are supercritical pitchfork bifurcations; the first is that of the symmetric steady solution of the flow, while the second is that of the limit cycle associated with the cyclic release of vortices in the wake of the cylinders. Since it is non-generic, this coincidence should not have been observed in the wake flow, and the literature on this coincidence is surprisingly sparse [17].

In this Letter, we model and explain in detail the non-generic coincidence of these two local pitchfork bifurcations in the fluidic pinball.

Flow configuration. – The fluidic pinball configuration consists of three fixed cylinders of diameter D whose axes are located at the vertices of an equilateral triangle of side $3D/2$ in the (x, y) plane and which are oriented perpendicularly to this plane. The domain is the rectangle $[-6D, 20D] \times [-6D, 6D]$. One vertex of the triangle points upstream and the midpoint of the back two cylinders is chosen as the origin. The upstream flow, of uniform velocity U_∞ at the input of the domain, is in the x direction. A variety of flow patterns is found in this configuration as the Reynolds number and spatial arrangement are

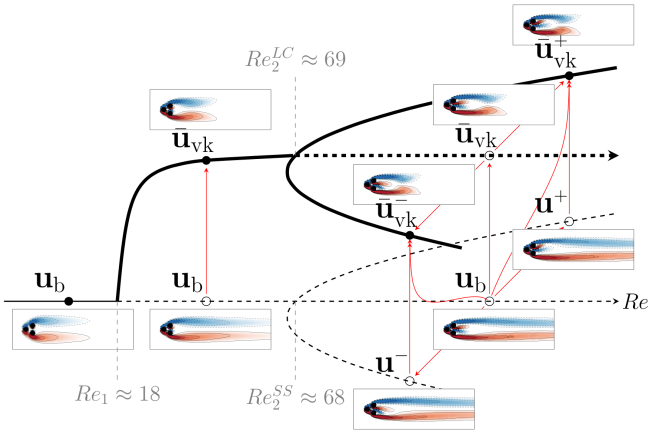

Fig. 1: Bifurcation diagram for the fluidic pinball. Solid curves indicate stable branches and dashed curves indicate unstable branches. Bold curves indicate branches of periodic solutions and thin curves indicate steady solutions. The symmetric and asymmetric periodic solutions are presented by their time-averages $\bar{\mathbf{u}}_{\rm vk}$ and $\bar{\mathbf{u}}_{\rm vk}^{\pm}$. Vorticity fields are color-coded in the range $[-1.5, 1.5]$ from blue to red. The red arrows show the possible transitions between them. The critical Reynolds numbers are detected with linear or Floquet stability analysis of the corresponding solutions.

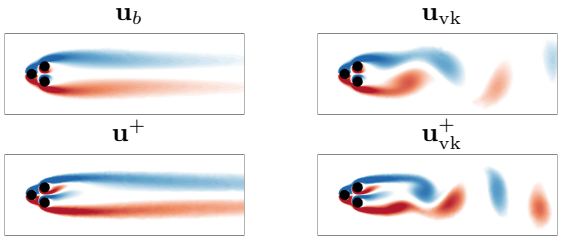

Fig. 2: Vorticity fields of the basic flow $\mathbf{u}_b$, a snapshot of the von Kármán vortex street $\mathbf{u}_{\rm vk}(t)$, at $Re = 30 > Re_1$, the asymmetric steady solution $\mathbf{u}^{+}$ and a snapshot of the asymmetric von Kármán vortex street $\mathbf{u}_{\rm vk}^{+}(t)$, , with the base-bleeding jet deflected to the top, at $Re = 80 > Re_2$, color-coded like in Fig. 1.

varied [18–20]. We solve the Navier-Stokes equations:

$$\partial_t \mathbf{u} + \nabla \cdot \mathbf{u} \otimes \mathbf{u} = \nu \triangle \mathbf{u} - \nabla p, \qquad (1)$$

using a second-order finite-element discretization method of the Taylor-Hood type [21], on an unstructured grid of 4 225 triangles and 8 633 vertices and implicit third-order time integration [22]. The Reynolds number is defined by $Re = U_\infty D/\nu$, where ν is the kinematic viscosity of the fluid. A no-stress condition is applied at the output of the domain.

Reflection symmetry in y proves to be an important part of this scenario. For a velocity field $\mathbf{u} = (u, v)$ we define the y-reflection operator R via $R(u, v)(x, y) \equiv (u, -v)(x, -y)$. For a symmetric field, u is even and v is odd in y. The spanwise vorticity $\partial_x v - \partial_y u$ used to represent the flows in our visualizations, manifests y-reflection symmetry by being odd in y. Eigenvectors obtained by linearizing about a reflection-symmetric state are necessarily either symmetric or antisymmetric. Antisymmetric eigenvectors are associated with pitchfork bifurcations that lead to two symmetrically related asymmetric branches if they are real. If they are complex conjugate pairs, they are associated with Hopf bifurcations that lead to limit cycles satisfying the spatio-temporal symmetry $R\mathbf{u}(t) = \mathbf{u}(t + T/2)$. Symmetric real eigenvectors are associated with transcritical bifurcations and complex conjugate eigenvectors are associated with Hopf bifurcations leading to limit cycles that remain symmetric throughout: $R\mathbf{u}(t) = \mathbf{u}(t)$.

The bifurcation diagram is sketched in Fig. 1. For low Reynolds number, there is a unique solution $\mathbf{u}_b$, called the basic flow. Depicted in Fig. 2(a), it is steady and reflection-symmetric with respect to $y = 0$. This solution undergoes a supercritical Hopf bifurcation at $Re_1 \approx 18$ to a pair of y-antisymmetric eigenmodes, leading to cyclic vortex shedding in the wake flow. The resulting T-periodic limit cycle, shown via the instantaneous visualization in Fig. 2(b), is the von Kármán vortex street and has the spatio-temporal symmetry $\mathbf{u}_{\rm vk}(t + T/2) = R\mathbf{u}_{\rm vk}(t)$ [23]. For this reason, we will call this limit cycle symmetric, despite the fact that the instantaneous flows are not symmetric.

At $Re = Re_2^{SS} \approx 68$, the basic flow undergoes another bifurcation, a supercritical pitchfork that breaks reflection symmetry by deflecting the base-bleeding jet up or down. Two asymmetric branches are generated: $\mathbf{u}^{+}$ with upwards deflection, shown in Fig. 2(c), and its y-reflection $\mathbf{u}^{-} = R\mathbf{u}^{+}$, with downwards deflection.

Like the steady basic flow, the periodic von Kármán vortex street $\mathbf{u}_{\rm vk}$ also undergoes a supercritical pitchfork bifurcation, also involving deflection of the base-bleeding jet, as shown in Fig. 2(d). This bifurcation occurs at $Re_2^{LC} \approx Re_2^{SS}$ and leads to two limit cycles $\mathbf{u}_{\rm vk}^{\pm}$ that we call asymmetric because they lack the spatio-temporal symmetry. Before symmetry breaking, the vortex shedding is initiated downstream after the stagnation point of the jet. After symmetry breaking, the vortex shedding is initiated behind one of the back two cylinders, and the stagnation point disappears.

Stability analysis. – In order to better understand this coincidence, we conducted linear stability analysis of the basic flow. As shown in Fig. 3(a), a real eigenvalue has crossed the imaginary axis at $Re_2^{SS} = 68 \pm 1$. We also performed Floquet analysis of the von Kármán vortex street. Fig. 3(b) shows that a Floquet multiplier $\lambda = e^{(\sigma + i\omega)T}$ crosses the unit circle at $+1$ and the critical value determined is $Re_2^{LC} = 69 \pm 1$, which is very close to Re_2^{SS}.

Fig. 4(a,b) show the deviation of the von Kármán vortex street from the base flow at $Re = 70 > Re_2$ at two instants separated by a quarter-period, together with the corresponding Floquet modes in Fig. 4(c,d). Fig. 4(e) is the eigenmode responsible for the pitchfork bifurcation of the

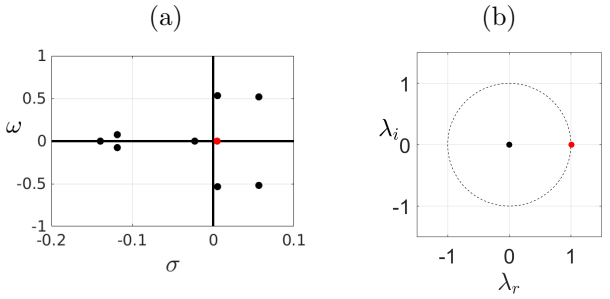

Fig. 3: (a) Leading eigenvalues of the basic flow and (b) leading Floquet multipliers of the von Kármán vortex street, both at $Re = 70$. Red circles mark the coincident eigenvalues.

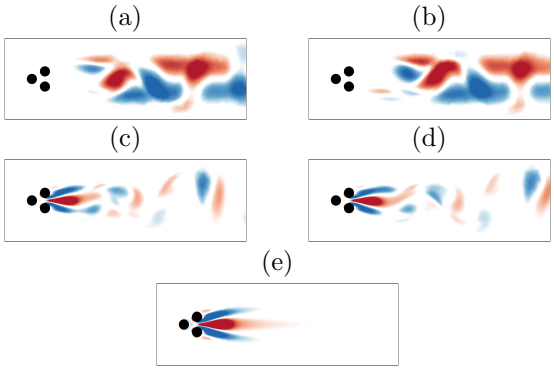

Fig. 4: (a, b) Deviation of the von Kármán vortex street from the base flow $\mathbf{u}_{\rm vk}(t) - \mathbf{u}_b$ at two instants separated by $T/4$, (c, d) the corresponding Floquet modes, and (e) the eigenmode with real eigenvalue of the basic flow, at $Re = 70$. For (a-d), the spatio-temporal symmetry $\mathbf{u}(t + T/2) = R\mathbf{u}(t)$ implies that the next two instants are obtained by y-reflection and sign change (color reversal) of these vorticity fields. In (e), the spanwise vorticity is even in y, corresponding to a flow which is antisymmetric with respect to y-reflection symmetry.

base flow. These correspond to the positive real eigenvalue of Fig. 3(a) and the Floquet multiplier crossing the unit circle at $= +1$ of Fig. 3(b). The spatial structures of these modes resemble one another, indicating that the two pitchfork bifurcations are closely related and correspond to the same physical mechanism, i.e. the base-bleeding jet which is dominant in the near wake throughout the development of the von Kármán vortex street. The pitchfork bifurcations originate locally within the three cylinders of the fluidic pinball mechanism, while the von Kármán vortex street originates in the wake of the three cylinders taken as a whole and approximated by a single obstacle. Fig. 4(a,b) shows that the difference between the von Kármán vortex street and the base flow is nearly zero near the three cylinders, which makes it plausible that both flows undergo the same local instability within the pinball mechanism.

The real eigenvalue of the basic flow $\mathbf{u}_b$ and the real part of the Floquet exponent $\sigma + i\omega$ of the von Kármán vortex street $\mathbf{u}_{\rm vk}$ are plotted in Fig. 5 as functions of the Reynolds number. The fact that the curves in Fig. 5 remain parallel confirms that the jet's instability mechanism is independent of the downstream flow. Both eigenvalues increase with Re, eventually causing both $\mathbf{u}_{\rm vk}$ and $\mathbf{u}_b$ to undergo symmetry-breaking pitchfork bifurcations at very close though distinct values of Re that deviate the central jet upwards or downwards.

A simple model for the coincidence. – We now write down a simple model for this phenomenon. Consider a system that undergoes successively a supercritical Hopf bifurcation and, for a higher value of the control parameter μ, a supercritical pitchfork bifurcation. In the fluidic pinball, μ is the Reynolds number Re. The system involves three degrees of freedom, the two that are involved in the Hopf bifurcation, written in polar form as $re^{i\theta}$ and that involved in the pitchfork, z. The generic form of such a system reads:

$$\begin{cases} \dot{r} &= (\mu - \mu_1 - r^2 - \chi_r z^2) r \\ \dot{\theta} &= \omega_0 + r^2 - \chi_i z^2 \\ \dot{z} &= (\mu - \mu_2 - z^2 - \chi_z r^2) z \end{cases} . \qquad (2)$$

The basic state $r = 0 = z$ undergoes a Hopf bifurcation at $\mu = \mu_1$, leading to a limit cycle with $r = \sqrt{\mu - \mu_1}$, $z = 0$, and a pitchfork bifurcation at $\mu = \mu_2$, leading to asymmetric steady states with $z = \pm\sqrt{\mu - \mu_2}$. Solutions with $r > 0$ and $z \neq 0$, i.e. asymmetric limit cycles, exist for $\mu > \mu_c$ where

$$\mu_c \equiv \mu_2 + \frac{\chi_z}{1 - \chi_z}(\mu_2 - \mu_1). \qquad (3)$$

If $\chi_z = 0$, then $\mu_c = \mu_2$, i.e. the pitchforks of the limit cycle and of the basic flow take place at the same critical value. and if $|\chi_z| \ll 1$, they occur almost simultaneously in μ. The non-generic property of coincident bifurcations is a direct consequence of $\chi_z \approx 0$.

The eigenvalues of system 2 are easily calculated from its Jacobian. The basic state has eigenvalues $\mu - \mu_1$ and $\mu - \mu_2$ in the r and z directions, respectively. The Floquet exponents of the symmetric limit cycle are the eigenvalues of system 2 with θ removed, that are $-2(\mu - \mu_1)$ and $\mu - \mu_2 - \chi_z(\mu - \mu_1)$. The second Floquet exponent will closely track eigenvalue $\mu - \mu_2$ of the basic flow, as in Fig. 5, if $|\chi_z(\mu - \mu_1)|$ remains small compared to μ_2.

Least-order Galerkin model for the coincidence. – We can derive system 2 from the corresponding least-order Galerkin model [16] slaving the Reynolds-stress-related modes. As stated there, the dynamics for $Re > Re_2$ requires at least a 5th order Galerkin expansion. The ansatz for the velocity field reads:

$$\mathbf{u}(\mathbf{x}, t) = \mathbf{u}_b(\mathbf{x}) + \sum_{i=1}^{5} a_i(t)\mathbf{u}_i(\mathbf{x}), \qquad (4)$$

where $\mathbf{u}_b(\mathbf{x})$ is the symmetric base flow of the Navier-Stokes equations. The elementary modes $\mathbf{u}_i(\mathbf{x})$ are shown

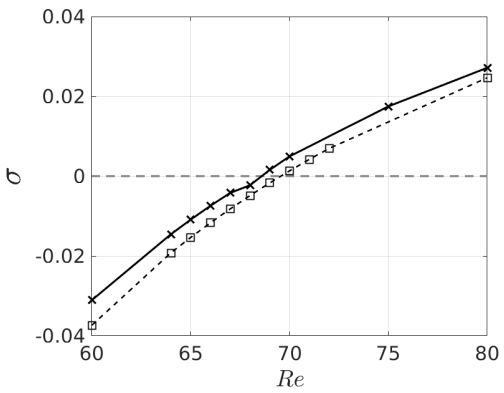

Fig. 5: Evolution of the real eigenvalue of the basic flow $\mathbf{u}_b$ (solid curve with crosses), and the real part of the Floquet exponent of the von Kármán vortex street $\mathbf{u}_{\rm vk}$ (dashed curve with squares) with the Reynolds number.

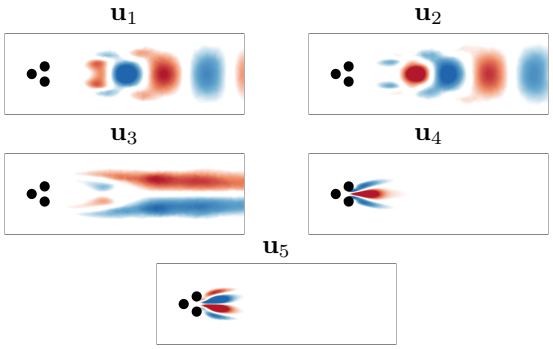

Fig. 6: Elementary modes of the fluidic pinball at $Re = 70$. See text for details.

in Fig. 6. Details on the identification of the individual modes can be found in [16].

The first two modes $\mathbf{u}_{1,2}$, associated with the vortex shedding, are taken to be the two leading modes from Proper Orthogonal Decomposition (POD) in the permanent dynamical flow regime [24]. The shift mode $\mathbf{u}_3$ is the difference between the mean flow $\bar{\mathbf{u}}_{\rm vk}$ of the periodic regime and the basic flow $\mathbf{u}_b$ [5]. Mode $\mathbf{u}_4$ is given by $\mathbf{u}_4 \propto \mathbf{u}^+ - \mathbf{u}^-$. Analogously to $\mathbf{u}_3$, mode $\mathbf{u}_5$ is the difference between the average $(\mathbf{u}^+ + \mathbf{u}^-)/2$ of the asymmetric steady solutions and the base flow $\mathbf{u}_b$.

The degrees of freedom a_1, a_2, a_4, are active, while a_3 and a_5 are slaved to a_1, a_2 and a_4. In the neighborhood of the second bifurcation threshold ($Re \approx Re_2$), the dynamical system reads:

$$da_1/dt = \sigma a_1 - \omega a_2, \qquad \sigma = \sigma_1 - \beta a_3 + \xi_r a_5 \quad (5)$$
$$da_2/dt = \sigma a_2 + \omega a_1, \qquad \omega = \omega_1 + \gamma a_3 + \xi_i a_5 \quad (6)$$
$$da_3/dt = \sigma_3 a_3 + \beta_3 \left(a_1^2 + a_2^2\right) \quad (7)$$
$$da_4/dt = \sigma_4 a_4 - \beta_4 a_4 a_5 + \xi_z a_4 a_3 \quad (8)$$
$$da_5/dt = \sigma_5 a_5 + \beta_5 a_4^2 \quad (9)$$

which is equivalent to the system 2 if $\sigma_3 \ll 0$ and $\sigma_5 \ll 0$. Indeed, if these conditions are satisfied, the slaved modes $a_3 \propto a_1^2 + a_2^2$ and $a_5 \propto a_4^2$ provide the cubic nonlinearities of Eq. 2 with $a_1 + i a_2 = r e^{i\theta}$ and $z \equiv a_4$. The coefficients of Eq. 5 can be directly computed by a Galerkin projection of the Navier-Stokes equations on the bifurcation modes $\mathbf{u}_{1\ldots5}$. At $Re = 70$, close to Re_2, $\chi_z = 0.0168$, confirming that it is small.

Discussion. – To check the robustness of the coincidence, we changed the distance between the cylinders from $L/D = 1.5$ to 1.4 and 1.6. The critical Reynolds numbers for the Hopf and pitchfork bifurcations, together with the associated χ_z, are recorded in Table 1. In all three cases, the two pitchfork bifurcations still closely coincide, confirming the robustness of this phenomenon with respect to a change in one of the control parameters (here the cylinder gap).

For these cases, the three cylinders work as a single bluff body. The base-bleeding jet focuses on the near flow, which breaks the symmetry but does not separate the bluff body wake. When L/D is sufficiently large, however, the three cylinders no longer form one compact body. Two vortex streets appear and compete with each other. A new mechanism then changes the flow dynamics completely with varying gap distance; we refer interested readers to [20].

We argue that coincident bifurcations like that observed in the fluidic pinball at $Re = Re_2$ should be observed in other flow configurations, and more generally in other nonlinear partial differential equations, when competing and independent instability mechanisms are present.

* * *

This work is supported by a public grant overseen by the French National Research Agency (ANR) by grant 'FlowCon' (ANR-17-ASTR-0022). N. D. has been supported by the China Scholarships Council (No.201808070123).

REFERENCES

[1] Strykowski P. and Sreenivasan K., *J. Fluid Mech.*, **218** (1990) 71.
[2] Crawford J. D. and Knobloch E., *Annu. Rev. Fluid Mech.*, **23** (1991) 341.
[3] Rowley C. W., Colonius T. and Basu A. J., *J. Fluid Mech.*, **455** (2002) 315.
[4] Dušek J., Le Gal P. and Fraunié P., *J. Fluid Mech.*, **264** (1994) 59.
[5] Noack B. R., Afanasiev K., Morzynski M., Tadmor G. and Thiele F., *J. Fluid Mech.*, **497** (2003) 335.
[6] Fabre D., Auguste F. and Magnaudet J., *Phys. Fluids*, **20** (2008) 051702.
[7] Dimitriadis G. and Li J., *AIAA Journal*, **47** (2009) 2577.
[8] Grandemange M., Cadot O. and Gohlke M., *Phys. Rev. E*, **86** (2012) 035302(R).

Table 1: Critical Reynolds numbers for the two bifurcations and associated χ_z when the cylinder gap is varied. For each gap, χ_z is determined from Galerkin projection close to the threshold at $Re = Re_2^{LC} + 1$.

L/D	Re_1	Re_2^{SS}	Re_2^{LC}	χ_z
1.4	18	79	80	0.0099
1.5	18	68	69	0.0168
1.6	20	63	63	0.0186

[9] Mizushima J. and Shiotani Y., *J. Fluid Mech.*, **434** (2001) 355.

[10] Mamun C. K. and Tuckerman L. S., *Phys. Fluids*, **7** (1995) 80.

[11] Smyth W. D. and Moum J. N., *Oceanography*, **25** (2012) 140.

[12] Grossmann S., Lohse D. and Sun C., *Annu. Rev. Fluid Mech.*, **48** (2016) .

[13] Schewe G., *J. Fluid Mech.*, **134** (1983) 311.

[14] Zhang H.-Q., Fey U., Noack B. R., König M. and Eckelmann H., *Phys. Fluids*, **7** (1995) 779.

[15] Henderson R. D. and Barkley D., *J. Fluid Mech.*, **322** (1996) 215.

[16] Deng N., Noack B. R., Morzyński M. and Pastur L. R., *J. Fluid Mech.*, **884** (2020) A37.

[17] Shearer M., *J. Math. Anal. Appl.*, **84** (1981) 113.

[18] Bao Y., Zhou D. and Huang C., *Comput Fluids*, **39** (2010) 882.

[19] Zheng S., Zhang W. and Lv X., *Comput Fluids*, **130** (2016) 94.

[20] Chen W., Ji C., Alam M. M., Williams J. and Xu D., *J. Fluid Mech.*, **891** (2020) 1.

[21] Taylor C. and Hood P., *Comput Fluids*, **1** (1973) 73.

[22] Noack B. R. and Morzyński M., Tech. Rep. Chair of Virtual Engineering, Poznan University of Technology, Poland 02/2017 (2017).

[23] Barkley D., *EPL (Europhysics Letters)*, **75** (2006) 750.

[24] Taira K., Brunton S. L., Dawson S. T., Rowley C. W., Colonius T., McKeon B. J., Schmidt O. T., Gordeyev S., Theofilis V. and Ukeiley L. S., *AIAA Journal*, **55** (2017) 4013.